IOPscience iopscience.iop.org

Home Search Collections Journals About Contact us My IOPscience

Strong-coupling theory of the interlayer tunnelling model for high-temperature superconductors

This article has been downloaded from IOPscience. Please scroll down to see the full text article.

1997 J. Phys.: Condens. Matter 9 9007

(http://iopscience.iop.org/0953-8984/9/42/015)

View the table of contents for this issue, or go to the journal homepage for more

Download details:
IP Address: 171.66.16.209
The article was downloaded on 14/05/2010 at 10:49

Please note that terms and conditions apply.

J. Phys.: Condens. Matter **9** (1997) 9007–9020. Printed in the UK PII: S0953-8984(97)83236-5

Strong-coupling theory of the interlayer tunnelling model for high-temperature superconductors

Božidar Mitrović and Melissa Castle

Physics Department, Brock University, St Catharines, Ont., Canada L2S 3A1

Received 8 April 1997, in final form 31 July 1997

Abstract. The interlayer pair tunnelling model of Anderson *et al* is generalized to include the strong-coupling effects associated with in-plane interactions. The equations for the superconducting transition temperature T_c are solved numerically for several models of electron–optical phonon coupling. The nonmagnetic in-plane impurity scattering suppresses the T_c in all cases considered, and it is possible to obtain a fair agreement with experiments for a reasonable choice of parameters. For the anisotropic electron–phonon coupling proposed by Song and Annett we find that the interlayer pair tunnelling can stabilize the $d_{x^2-y^2}$-wave superconducting state with a high T_c. Moreover, in this case there is a possibility of impurity-induced crossover from the $d_{x^2-y^2}$-wave state stabilized by the interlayer tunnelling to the s-wave state at a low impurity concentration. We also calculate the isotope effect associated with the in-plane oxygen optical mode and its dependence on the strength of the interlayer pair tunnelling. Small positive values of the isotope exponent are obtained for strengths of pair tunnelling that give high transition temperatures.

1. Introduction

One of the theories proposed for high-T_c copper oxide superconductors is the interlayer pair tunnelling (ILPT) model first suggested by Wheatly, Hsu and Anderson [1] and refined by Chakravarty, Sudbø, Anderson and Strong [2–5]. In the ILPT model the pairing in the individual copper–oxygen layers is enhanced and sustained by the pair tunnelling between the layers within the unit cell. The symmetry of the component of the order parameter resulting from in-plane interactions is not an essential feature of the model, although in the original work [2] it was assumed that this component has s-wave symmetry. In this paper we generalize the BCS-like form of the ILPT model given by Chakravarty *et al* to include the retardation (i.e. the strong-coupling) effects resulting from in-plane interactions. This generalization is necessary in order to obtain a more realistic dependence of T_c and other quantities characterizing the superconducting state on the interaction parameters [6]. Moreover, the strong-coupling form of the interlayer pair tunnelling model is suitable for including the effect of in-plane nonmagnetic impurity scattering. The dependence of T_c on impurity concentration [7–10] is considered to be an important indicator of the symmetry of the order parameter in oxide superconductors and of the underlying pairing mechanism [11, 12].

As in [2–5], we assume that in the superconducting state the quasiparticle picture is approximately valid. This point has been taken in [2], based on photoemission experiments. It should be kept in mind, however, that Chakravarty and Anderson [13] attempted an indirect justification of the pair tunnelling Hamiltonian based on a non-Fermi-liquid form

0953-8984/97/429007+14$19.50 © 1997 IOP Publishing Ltd

of the normal-state electron propagator. Sudbø [14] considered the effects of a non-Fermi-liquid form of the diagonal part of the electron propagator in the superconducting state on the intralayer pair susceptibility. Since the starting assumptions in [13] and [14] are as phenomenological as the pair tunnelling Hamiltonian of [2–5], and since the experiments seem to suggest that in the superconducting state the quasiparticle picture is recovered, we will proceed as in [2–5] and assume that both the diagonal and the off-diagonal part of the electron self-energy can be obtained from the relevant interactions using the standard second-order self-consistent perturbation theory. The self-energy equations derived in this paper are valid for any kind of in-plane pairing interaction within the one-boson exchange approximation. In our numerical work, however, we consider only the case in which the in-plane pairing arises from electron coupling to optical phonons. This was motivated by the fact that the ILPT mechanism is novel enough that its consequences should be examined first when the in-plane pairing is caused by the conventional electron–phonon interaction before more exotic in-plane interaction models are considered. Also, Song and Annett [15] recently derived an effective single-band Hubbard-type Hamiltonian for CuO_2 planes which includes the electron–phonon coupling to oxygen breathing modes. The electron–phonon matrix element squared is proportional to $\sin^2((k_x - k'_x)/2) + \sin^2((k_y - k'_y)/2)$, where $\boldsymbol{k}$ and $\boldsymbol{k}'$ are the electron momenta. With this form of coupling Song and Annett initially predicted that the order parameter with $d_{x^2-y^2}$-wave symmetry leads to a higher transition temperature than the order parameter with s-wave symmetry, because in the former case the on-site Coulomb repulsion U becomes ineffective. Subsequently, they found this conclusion to be erroneous, which we independently confirmed during the course of this study. We found, however, that the $d_{x^2-y^2}$-wave state could be stabilized by the interlayer tunnelling.

In the numerical work we concentrate on the superconducting transition temperature and examine whether the ILPT model can explain the observed suppression of T_c with increasing impurity concentration [7–10], as well as the observed small values of the oxygen isotope effect in high-T_c superconductors.

The rest of the paper is organized as follows. In section 2 we give in some detail the derivation of the interlayer tunnelling contribution to the electron self-energy in the superconducting state and list the well known results for the self-energy parts arising from in-plane interactions. In addition, we summarize the T_c-equations for the case of pairing induced by electron–optical phonon coupling. Section 3 contains our numerical results for the transition temperature as a function of disorder and the oxygen isotope exponent, and finally in section 4 we give conclusions.

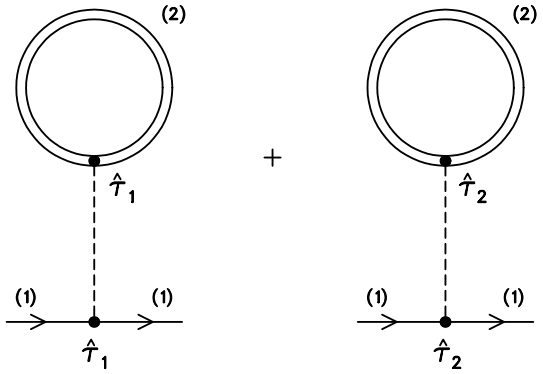

Figure 1. The interlayer pair tunnelling contribution to the electron Nambu self-energy.

2. Theory

2.1. Self-energy due to interlayer pair tunnelling

In the ILPT model it is assumed that in the superconducting state the quasiparticle picture is approximately valid for motion within a layer, while the coherent motion of quasiparticles from layer to layer within the unit cell is blocked [2, 3]. The part of the Hamiltonian which describes the interlayer pair tunnelling for two layers per unit cell [2, 5] is

$$H_J = -\sum_{\boldsymbol{k}} T_J(\boldsymbol{k})[c^{(1)\dagger}_{\boldsymbol{k}\uparrow} c^{(1)\dagger}_{-\boldsymbol{k}\downarrow} c^{(2)}_{-\boldsymbol{k}\downarrow} c^{(2)}_{\boldsymbol{k}\uparrow} + \text{HC}] \tag{1}$$

where $c^{(i)\dagger}_{\boldsymbol{k}\uparrow}$ is an electron creation operator for the state of two-dimensional momentum $\boldsymbol{k}$ and spin $\uparrow$ in the layer i, and

$$T_J(\boldsymbol{k}) = \frac{t_\perp^2}{16t}[\cos(k_x a) - \cos(k_y a)]^4 \tag{2}$$

as suggested by band-structure calculations [16]. Here, $t_\perp$ characterizes the high-energy single-electron coherent hopping from layer to layer, and is estimated to be between 0.1 eV and 0.15 eV [2]. The parameter t enters the tight-binding dispersion for the electron motion within a layer:

$$\varepsilon_{\boldsymbol{k}} = -2t[\cos(k_x a) + \cos(k_y a)] - 4t' \cos(k_x a)\cos(k_y a) - \mu \tag{3}$$

where μ is the chemical potential and a is the lattice constant. To find the contribution to the anomalous electron self-energy from the Hamiltonian (1), it is convenient to rewrite the Hamiltonian in the Nambu formalism [17]. Introducing the Nambu fields

$$\Psi^{(i)}_{\boldsymbol{k}} = \begin{pmatrix} c^{(i)}_{\boldsymbol{k}\uparrow} \\ c^{(i)\dagger}_{-\boldsymbol{k}\downarrow} \end{pmatrix} \qquad \Psi^{(i)\dagger}_{\boldsymbol{k}} = (c^{(i)\dagger}_{\boldsymbol{k}\uparrow} c^{(i)}_{-\boldsymbol{k}\downarrow})$$

the Hamiltonian (1) could be written as

$$H_J = -\sum_{\boldsymbol{k}} \frac{T_J(\boldsymbol{k})}{2}[\Psi^{(1)\dagger}_{\boldsymbol{k}} \hat{\tau}_1 \Psi^{(1)}_{\boldsymbol{k}} \Psi^{(2)\dagger}_{\boldsymbol{k}} \hat{\tau}_1 \Psi^{(2)}_{\boldsymbol{k}} + \Psi^{(1)\dagger}_{\boldsymbol{k}} \hat{\tau}_2 \Psi^{(1)}_{\boldsymbol{k}} \Psi^{(2)\dagger}_{\boldsymbol{k}} \hat{\tau}_2 \Psi^{(2)}_{\boldsymbol{k}}] \tag{4}$$

where $\hat{\tau}_1$ and $\hat{\tau}_2$ are the two off-diagonal Pauli matrices [17]. This expression looks like the sum of two two-body interaction Hamiltonians with the interaction line $-T_J(\boldsymbol{k})\delta_{\boldsymbol{k},\boldsymbol{k}'}\delta_{\boldsymbol{q},0}$ and with the interaction vertices $\hat{\tau}_1$ and $\hat{\tau}_2$, respectively [17]. Since the ILPT model does not consider the correlations of the type $-\langle T_\tau(\Psi^{(1)}_{\boldsymbol{k}}(\tau)\Psi^{(2)\dagger}_{\boldsymbol{k}}(0))\rangle$, where T_τ is Wick's time-ordering operator, we consider only the contribution to the electron Nambu self-energy arising from the Hartree-type diagrams shown in figure 1. The contribution of these two diagrams to the irreducible Nambu electron self-energy in layer (1) is

$$\hat{\Sigma}^{(1)}_J(\boldsymbol{k}) = -\frac{T_J(\boldsymbol{k})}{2} T \sum_m \left[\hat{\tau}_1 \operatorname{Tr}\{\hat{\tau}_1 \hat{G}^{(2)}(\boldsymbol{k}, \mathrm{i}\omega_m)\} + \hat{\tau}_2 \operatorname{Tr}\{\hat{\tau}_2 \hat{G}^{(2)}(\boldsymbol{k}, \mathrm{i}\omega_m)\}\right] \tag{5}$$

where T is the temperature in energy units, $\hat{G}^{(2)}(\boldsymbol{k}, \mathrm{i}\omega_m)$ is the Nambu 2×2 electron Green's function for layer (2) at wave vector $\boldsymbol{k}$ and the fermion Matsubara frequency $\mathrm{i}\omega_m$, $\operatorname{Tr}\{\cdots\}$ is the trace, and the overall minus sign arises from one closed fermion loop. With the usual form for the *total* irreducible electron Nambu self-energy in layer i,

$$\hat{\Sigma}^{(i)}(\boldsymbol{k}, \mathrm{i}\omega_n) = \mathrm{i}\omega_n(1 - Z^{(i)}(\boldsymbol{k}, \mathrm{i}\omega_n))\hat{\tau}_0 + \phi^{(i)}(\boldsymbol{k}, \mathrm{i}\omega_n)\hat{\tau}_1 + \bar{\phi}^{(i)}(\boldsymbol{k}, \mathrm{i}\omega_n)\hat{\tau}_2 + \chi^{(i)}(\boldsymbol{k}, \mathrm{i}\omega_n)\hat{\tau}_3 \tag{6}$$

where $Z^{(i)}$ is the renormalization function, $\phi^{(i)}$ and $\bar{\phi}^{(i)}$ are the real and imaginary parts, respectively, of the pairing self-energy, and $\chi^{(i)}$ is the part of diagonal self-energy which is even in $i\omega_n$, equation (5) takes the form

$$\hat{\Sigma}_J^{(1)}(\boldsymbol{k}) = T_J(\boldsymbol{k})T\sum_m \frac{\phi^{(2)}(\mathrm{KI})\hat{\tau}_1 + \bar{\phi}^{(2)}(\mathrm{KI})\hat{\tau}_2}{(\omega_m Z^{(2)}(\mathrm{KI}))^2 + (\varepsilon_{\boldsymbol{k}}^{(2)} + \chi^{(2)}(\mathrm{KI}))^2 + |\phi^{(2)}(\mathrm{KI}) + i\bar{\phi}^{(2)}(\mathrm{KI})|^2} \tag{7}$$

(in this equation, (KI) stands for $(\boldsymbol{k}, i\omega_m)$ for convenience of layout). It should be noted that the interlayer pair tunnelling does not lead to any frequency dependence in the self-energy, but contributes directly only to the pairing (i.e. off-diagonal) self-energy and, as emphasized in [2], the resulting self-energy is local in $\boldsymbol{k}$. Moreover, in the weak-coupling approximation for in-plane interactions $Z^{(2)} = 1$, $\chi^{(2)} = 0$ and $\phi^{(2)}$ and $\bar{\phi}^{(2)}$ do not depend on the Matsubara frequency, and the sum in (7) could be easily performed using contour integration [17]. One finds

$$\hat{\Sigma}_J^{(1)}(\boldsymbol{k}) = T_J(\boldsymbol{k})(\phi^{(2)}(\boldsymbol{k})\hat{\tau}_1 + \bar{\phi}^{(2)}(\boldsymbol{k})\hat{\tau}_2)\frac{1}{E_{\boldsymbol{k}}}\tanh\left(\frac{E_{\boldsymbol{k}}}{2T}\right) \tag{8}$$

where $E_{\boldsymbol{k}} = \sqrt{(\varepsilon_{\boldsymbol{k}}^{(2)})^2 + |\phi^{(2)}(\boldsymbol{k}) + i\bar{\phi}^{(2)}(\boldsymbol{k})|^2}$, which is the same result (with $\bar{\phi}^{(2)}$ gauged away) as that obtained by Chakravarty, Sudbø, Anderson and Strong [2].

2.2. The self-energy due to in-plane interactions

The precise form of the self-energy due to in-plane interactions depends on the model used, and we will restrict ourselves to the case where the pairing interaction is due to one-boson (e.g. phonon or spin-fluctuation) exchange. The electron–phonon contribution to the self-energy is [17, 6, 18]

$$\hat{\Sigma}_{ep}^{(i)}(\boldsymbol{k}, i\omega_n) = -\frac{T}{N^2}\sum_{\boldsymbol{k}',\lambda,m} |g_{\boldsymbol{k}-\boldsymbol{k}',\lambda}|^2 D_\lambda(\boldsymbol{k}-\boldsymbol{k}', i\omega_n - i\omega_m)\hat{\tau}_3\hat{G}^{(i)}(\boldsymbol{k}', i\omega_m)\hat{\tau}_3 \tag{9}$$

where N^2 is the number of lattice sites, $g_{\boldsymbol{k}-\boldsymbol{k}',\lambda}$ is the electron–phonon matrix element for the momentum transfer $\boldsymbol{k}-\boldsymbol{k}'$ and the phonon polarization λ, $D_\lambda(\boldsymbol{k}-\boldsymbol{k}', i\nu_m)$ is the corresponding phonon propagator at the boson Matsubara frequency $i\nu_m$, and $\hat{G}^{(i)}$ is the electron propagator for the layer i. An analogous expression is obtained for the self-energy due to the exchange of antiferromagnetic spin fluctuations, except that $|g|^2D$ is replaced by the spin-fluctuation propagator and the Pauli matrix $\hat{\tau}_3$ by the unit 2×2 matrix [19].

In the case of phonon-mediated superconductivity one can include the effect of short-range Coulomb repulsion within an effective single-band Hubbard model for copper–oxygen planes [15]. The resulting contribution to the electron self-energy is

$$\hat{\Sigma}_c^{(i)} = -U\frac{T}{N^2}\sum_{\boldsymbol{k}',m}\hat{\tau}_3\hat{G}_{od}^{(i)}(\boldsymbol{k}', i\omega_m)\hat{\tau}_3 \tag{10}$$

where U is the on-site Coulomb repulsion and $\hat{G}_{od}^{(i)}$ is the off-diagonal part of the electron Nambu Green's function [18].

Finally we consider the effect of in-plane electron–impurity scattering. We will not consider all of the possible effects of electron–impurity scattering in two-dimensional superconductors (e.g. the enhancement of the Coulomb repulsion [20]), but will confine ourselves to the simplest treatment using either the second Born approximation or the t-matrix approximation. In the second Born approximation and assuming a constant electron–

impurity matrix element $V_i = \langle \boldsymbol{k}|V_N|\boldsymbol{k}'\rangle$, where V_N is the change in the crystal potential due to nonmagnetic impurity, the electron self-energy resulting from scattering off impurities is

$$\hat{\Sigma}_i(\mathrm{i}\omega_n) = \frac{n_i V_i^2}{N^2}\sum_{\boldsymbol{k}} \hat{\tau}_3 \hat{G}^{(i)}(\boldsymbol{k}, \mathrm{i}\omega_n)\hat{\tau}_3 \tag{11}$$

while in the t-matrix approximation the self-energy is given by

$$\hat{\Sigma}_i(\mathrm{i}\omega_n) = \frac{n_i V_i^2}{N^2}\sum_{\boldsymbol{k}} \hat{\tau}_3 \hat{G}^{(i)}(\boldsymbol{k}, \mathrm{i}\omega_n)\hat{\tau}_3 \left[\hat{\tau}_0 - \frac{V_i}{N^2}\sum_{\boldsymbol{k}} \hat{G}^{(i)}(\boldsymbol{k}, \mathrm{i}\omega_n)\hat{\tau}_3\right]^{-1}. \tag{12}$$

2.3. T_c-equations for the case of pairing due to electron–optical phonon coupling

We consider the case where the in-plane pairing is mediated by an optical phonon of energy Ω_E. Near T_c the pairing self-energies become infinitesimal and the self-energy equations could be linearized as described, for example, in [18, 19]. Assuming that the electron self-energies in each of the two layers are identical (e.g. $\phi^{(1)}(\boldsymbol{k}, \mathrm{i}\omega_n) = \phi^{(2)}(\boldsymbol{k}, \mathrm{i}\omega_n) = \phi(\boldsymbol{k}, \mathrm{i}\omega_n)$) and defining

$$u(\boldsymbol{k}, n) = \frac{\phi(\boldsymbol{k}, \mathrm{i}\omega_n)}{\sqrt{(\omega_n Z(\boldsymbol{k}, \mathrm{i}\omega_n))^2 + (\varepsilon_{\boldsymbol{k}} + \chi(\boldsymbol{k}, \mathrm{i}\omega_n))^2}} \tag{13}$$

the T_c-equation reduces to the eigenvalue problem of a real symmetric matrix:

$$u(\boldsymbol{k}, n) = \sum_{\boldsymbol{k}', m} K(\boldsymbol{k}, n; \boldsymbol{k}', m)u(\boldsymbol{k}', m). \tag{14}$$

The matrix K consists of several parts associated with various interactions:

$$K = K_{ep} + K_J + K_c + K_i. \tag{15}$$

The electron–phonon contribution is

$$K_{ep}(\boldsymbol{k}, n; \boldsymbol{k}', m) = \frac{T}{N^2}\sum_{\lambda} \left|g_{\boldsymbol{k},\boldsymbol{k}',\lambda}\right|^2 \frac{2\Omega_E}{(\omega_n - \omega_m)^2 + \Omega_E^2} S(\boldsymbol{k}, n)S(\boldsymbol{k}', m) \tag{16}$$

where

$$S(\boldsymbol{k}, n) = \frac{1}{\sqrt{(\omega_n Z(\boldsymbol{k}, \mathrm{i}\omega_n))^2 + (\varepsilon_{\boldsymbol{k}} + \chi(\boldsymbol{k}, \mathrm{i}\omega_n))^2}}. \tag{17}$$

The interlayer pair tunnelling contribution is

$$K_J(\boldsymbol{k}, n; \boldsymbol{k}', m) = \delta_{\boldsymbol{k},\boldsymbol{k}'} T T_J(\boldsymbol{k}')S(\boldsymbol{k}, n)S(\boldsymbol{k}', m) \tag{18}$$

while the contribution due to on-site Coulomb repulsion is

$$K_c(\boldsymbol{k}, n; \boldsymbol{k}', m) = -\frac{T}{N^2} U S(\boldsymbol{k}, n)S(\boldsymbol{k}', m). \tag{19}$$

Treating the in-plane impurity scattering in the second Born approximation gives

$$K_i(\boldsymbol{k}, n; \boldsymbol{k}', m) = \frac{n_i V_i^2}{N^2}\delta_{n,m} S(\boldsymbol{k}, n)S(\boldsymbol{k}', m) \tag{20}$$

while the t-matrix approximation gives

$$K_i(\boldsymbol{k}, n; \boldsymbol{k}', m) = \frac{n_i V_i^2}{N^2}\delta_{n,m} S(\boldsymbol{k}, n)S(\boldsymbol{k}', m)/D(n) \tag{21}$$

where

$$D(n) = \left\{ \left[1 + \frac{V_i}{N^2} \sum_{\boldsymbol{q}} (\varepsilon_{\boldsymbol{q}} + \chi(\boldsymbol{q}, \mathrm{i}\omega_n)) S(\boldsymbol{q}, n)^2 \right]^2 + \left[\frac{V_i}{N^2} \sum_{\boldsymbol{q}} \omega_n Z(\boldsymbol{q}, \mathrm{i}\omega_n) S(\boldsymbol{q}, n)^2 \right]^2 \right\}. \tag{22}$$

At a given temperature the functions $Z(\boldsymbol{k}, \mathrm{i}\omega_n)$, $\chi(\boldsymbol{k}, \mathrm{i}\omega_n)$ and the chemical potential μ (see equation (3)) are determined self-consistently by solving a set of equations:

$$Z(\boldsymbol{k}, \mathrm{i}\omega_n) = 1 + Z_{ep}(\boldsymbol{k}, \mathrm{i}\omega_n) + Z_i(\boldsymbol{k}, \mathrm{i}\omega_n) \tag{23}$$

$$\chi(\boldsymbol{k}, \mathrm{i}\omega_n) = \chi_{ep}(\boldsymbol{k}, \mathrm{i}\omega_n) + \chi_i(\boldsymbol{k}, \mathrm{i}\omega_n) \tag{24}$$

together with the equation representing the particle number conservation [21]:

$$n = \frac{1}{2} + \frac{2T}{N^2} \sum_{\boldsymbol{k}} \sum_{n=1}^{\infty} \mathrm{Re}\{G_{1,1}(\boldsymbol{k}, \mathrm{i}\omega_n)\} = \frac{1}{2} - \frac{2T}{N^2} \sum_{\boldsymbol{k}} \sum_{n=1}^{\infty} (\varepsilon_{\boldsymbol{k}} + \chi(\boldsymbol{k}, \mathrm{i}\omega_n)) S(\boldsymbol{k}, n)^2 \tag{25}$$

where n is the band filling factor and $G_{1,1}$ is the $(1, 1)$ component of the electron Nambu Green's function. In equations (23) and (24), Z_{ep} and χ_{ep} are given by

$$Z_{ep}(\boldsymbol{k}, \mathrm{i}\omega_n) = \frac{T}{\omega_n N^2} \sum_{\boldsymbol{k}', m} \sum_{\lambda} \left| g_{\boldsymbol{k}, \boldsymbol{k}', \lambda} \right|^2 \frac{2\Omega_E}{(\omega_n - \omega_m)^2 + \Omega_E^2} \omega_m Z(\boldsymbol{k}, \mathrm{i}\omega_m) S(\boldsymbol{k}', \mathrm{i}\omega_m)^2 \tag{26}$$

$$\chi_{ep}(\boldsymbol{k}, \mathrm{i}\omega_n) = -\frac{T}{N^2} \sum_{\boldsymbol{k}', m} \frac{2\Omega_E}{(\omega_n - \omega_m)^2 + \Omega_E^2} (\varepsilon_{\boldsymbol{k}'} + \chi(\boldsymbol{k}', \mathrm{i}\omega_m)) S(\boldsymbol{k}', m)^2 \tag{27}$$

while Z_i and χ_i are given by

$$Z_i(\boldsymbol{k}, \mathrm{i}\omega_n) = \frac{n_i V_i^2}{N^2} \sum_{\boldsymbol{k}'} Z(\boldsymbol{k}', \mathrm{i}\omega_n) S(\boldsymbol{k}', n)^2 \tag{28}$$

$$\chi_i(\boldsymbol{k}, \mathrm{i}\omega_n) = -\frac{n_i V_i^2}{N^2} \sum_{\boldsymbol{k}'} (\varepsilon_{\boldsymbol{k}'} + \chi(\boldsymbol{k}', \mathrm{i}\omega_n)) S(\boldsymbol{k}', n)^2 \tag{29}$$

in the second Born approximation, and by

$$Z_i(\boldsymbol{k}, \mathrm{i}\omega_n) = \frac{n_i V_i^2}{D(n) N^2} \sum_{\boldsymbol{k}'} Z(\boldsymbol{k}', \mathrm{i}\omega_n) S(\boldsymbol{k}', n)^2 \tag{30}$$

$$\chi_i(\boldsymbol{k}, \mathrm{i}\omega_n) = -\frac{n_i V_i^2}{D(n)} \left[V_i \left(\frac{1}{N^2} \sum_{\boldsymbol{q}} \omega_n Z(\boldsymbol{q}, \mathrm{i}\omega_n) S(\boldsymbol{q}, n)^2 \right)^2 + \frac{1}{N^2} \sum_{\boldsymbol{q}} (\varepsilon_{\boldsymbol{q}} + \chi(\boldsymbol{q}, \mathrm{i}\omega_n)) \right.$$
$$\left. \times S(\boldsymbol{q}, n)^2 \left(1 + \frac{V_i}{N^2} \sum_{\boldsymbol{q}} (\varepsilon_{\boldsymbol{q}} + \chi(\boldsymbol{q}, \mathrm{i}\omega_n)) S(\boldsymbol{q}, n)^2 \right) \right] \tag{31}$$

in the t-matrix approximation. The transition temperature T_c is determined as the highest temperature at which the largest eigenvalue of matrix K is equal to 1 (see equation (14)).

3. Numerical results

In the numerical calculations we have taken (for definiteness) the same band parameters as those in the work of Chakravarty *et al*, namely $t = 0.25$ eV and $t'/t = -0.45$. The band filling factor was set at $n = 0.375$ corresponding to 0.75 electrons per cell. In figure 2 we show the density of states $N(E)$ for these parameters obtained by adapting the tetrahedron

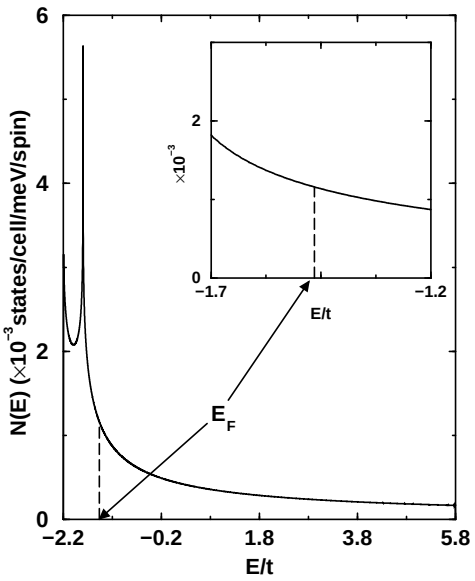

Figure 2. The electronic band density of states for the dispersion given by equation (3) calculated for a 400×400 lattice using the tetrahedron method. The energy is measured in units of t, and E_F indicates the Fermi level. The inset shows the density of states (using the same units) in the interval $[E_F - \Omega_E, E_F + \Omega_E]$, where $\Omega_E = 62$ meV is the energy of the optical phonon.

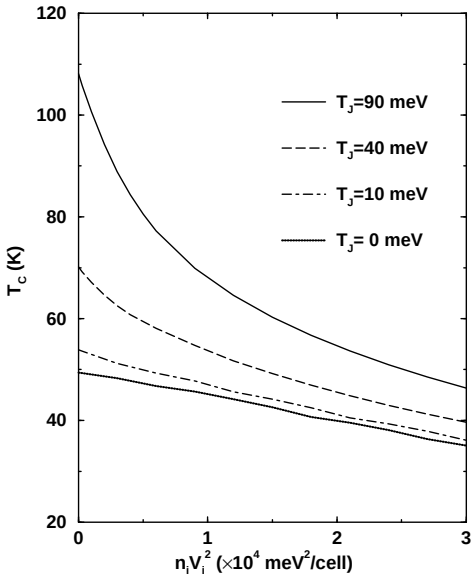

Figure 3. The dependence of T_c on $n_i V_i^2$, where n_i is the concentration of in-plane impurities and V_i is the electron–impurity matrix element, calculated in the Born approximation, equation (11), for several values of the interlayer pair tunnelling strength $T_J = t_\perp^2/t$, assuming the isotropic electron–phonon coupling model (32) ($\lambda = 0.48$), s-wave pairing, and the on-site Coulomb repulsion $U = 0$.

method [22] to a 400×400 square lattice. We assumed that the electrons couple to an optical phonon at energy $\Omega_E = 62$ meV (i.e. 500 cm^{-1}) [15], which corresponds roughly to the energy scale of the oxygen modes in high-T_c superconductors. Two models for the electron–phonon matrix element were considered. In the first model, which we will refer to as the isotropic model, a momentum-independent $\left|g_{\boldsymbol{k},\boldsymbol{k}',\lambda}\right|^2$ was assumed:

$$\sum_\lambda \left|g_{\boldsymbol{k},\boldsymbol{k}',\lambda}\right|^2 = |g|^2 \tag{32}$$

and the value of $|g|^2$ was chosen such that the electron–phonon mass renormalization parameter $\lambda \approx 0.5$. In the second model, which we will refer to as the anisotropic model, the momentum dependence of $\left|g_{\boldsymbol{k},\boldsymbol{k}',\lambda}\right|^2$ was taken to have the form given by Song and Annett [15]:

$$\sum_\lambda \left|g_{\boldsymbol{k},\boldsymbol{k}',\lambda}\right|^2 = \frac{|g|^2}{2}\left[\sin^2\left(\frac{k_x - k'_x}{2}\right) + \sin^2\left(\frac{k_y - k'_y}{2}\right)\right] \tag{33}$$

with the same value of $|g|^2$ as in (32), so the maximum in (33) is equal to $|g|^2$ in the isotropic model. Because the interlayer pair tunnelling contribution to the kernel in the T_c-equation (14) is local in $\boldsymbol{k}$, equation (19), the calculations had to be performed in $\boldsymbol{k}$-space except when considering an isotropic in-plane interaction with $T_J = 0$. In this case it is possible to convert the $\boldsymbol{k}$-sums into integrals over the electron energies and use the electronic density of states calculated for a large (400×400) lattice. The results for $T_J = 0$ and isotropic in-plane interaction served as a check of the accuracy of the results obtained from the calculations

in $\boldsymbol{k}$-space. Due to memory size restrictions on the computers that were available to us (4 processor SGI R4400 and Fujitsu VPX240/10) the largest lattice size that we could consider was 64×64. We found that it is absolutely critical to add and subtract the noninteracting form of the band filling factor n to the expression given as equation (25) and to evaluate the added part as $\int \mathrm{d}E\ N(E)/(\exp((E-\mu)/T)+1)$. Otherwise, the truncation of the sum over the Matsubara frequencies in (25) and the finite lattice size could lead to an error in T_c as great as 55% in the case of isotropic in-plane interaction with $T_J = 0$. This error in T_c is largely due to error in the chemical potential μ which leads to an incorrect value for the density of states near μ. We found that this trick of adding and subtracting leads to values of T_c that are accurate to better than 5% for the largest lattice size that we could consider. The largest eigenvalue of matrix K in (14) was obtained using the power method [23] and, due to the simple structure of the sums over the Matsubara frequencies in (25)–(31), there was no need to use the fast-Fourier-transform technique of Serene and Hess [24]. The resulting code vectorized 93–97% on Fujitsu VPX240/10.

3.1. T_c-suppression by in-plane impurity scattering

We first consider the isotropic model of electron–phonon interaction and, naturally, assume the s-wave symmetry of the pairing self-energy. Figure 3 illustrates the suppression of T_c by in-plane impurity scattering obtained within the Born approximation for four different values of the interlayer pair tunnelling parameter $T_J = t_\perp^2/t$ (equation (2)), and with the on-site Coulomb repulsion $U = 0$. It should be stated from the outset that with the strong-coupling effects (i.e. renormalization) one needs a larger value of T_J to achieve a transition temperature of about 100 K, typical of high-T_c superconductors with no disorder than in the BCS-like treatment [2, 25] (here the electron–phonon mass renormalization parameter is $\lambda = 0.48$ as deduced from the value of Z at the first Matsubara frequency and $\Omega_E = 62$). In the Born approximation the impurity scattering is parametrized by $n_i V_i^2$, and we plot T_c as a function of this quantity. If we take $1/2\tau_i \equiv \pi N(E_F) n_i V_i^2$, where $N(E_F)$ is the band electronic density of states at the Fermi level, as the measure of the elastic scattering rate, the range shown in figure 3 corresponds to about 110 meV; with $V_i = t = 250$ meV the maximum value of $n_i V_i^2$ in figure 3 is obtained for the in-plane impurity concentration $n_i = 0.48$ per cell. The overall shapes of the curves in figure 3 are similar to the results obtained by Bang [25] in the BCS-type treatment using the circular Fermi surface and $T_J(\boldsymbol{k}) \propto |\cos 2\phi|$, where ϕ gives the position of $\boldsymbol{k}$ on the Fermi surface. However, we find that T_c is suppressed at a much slower rate than that obtained by Bang in the Born limit [25]. At first, it is surprising that we get a drop in T_c with increasing $n_i V_i^2$ for $T_J = 0$. In this case there is no gap anisotropy which could be washed out by the impurity scattering leading to the suppression of T_c. Also, the structure in $N(E)$ within a range $\pm\Omega_E$ around the Fermi level does not seem to be significant enough (see the inset in figure 2) for the smearing caused by the elastic scattering rate $1/2\tau_i = \mathrm{O}(\Omega_E)$ to have any significant effect on T_c. We checked the result for $T_J = 0$ by converting the $\boldsymbol{k}$-sums into integrals over electronic energies, as discussed at the beginning of this section, and found the same result. Upon inspection we found that with increasing $n_i V_i^2$ there is a slight shift in the chemical potential to the region of lower density of states. Although the reduction of the density of states at the chemical potential is small, the exponential dependence of T_c on the interaction parameters presumably leads to the observed decrease in T_c for $T_J = 0$. Note that the rate of suppression is greater for increased T_J. The reason for this has been discussed by Bang [25].

Next we consider the effect of in-plane disorder in the t-matrix approximation. The

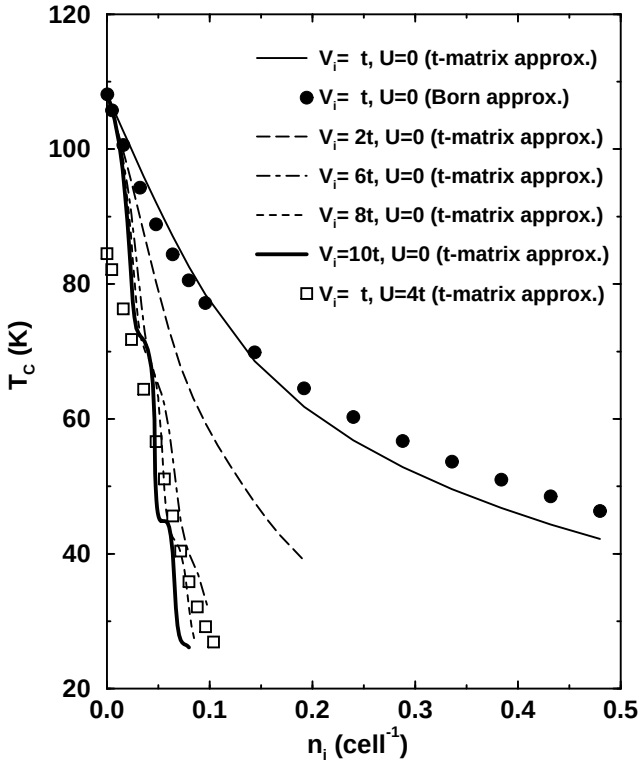

Figure 4. The dependence of T_c on the concentration n_i of in-plane impurities for the isotropic electron–phonon coupling model (32) ($\lambda = 0.48$) and $T_J = 90$ meV calculated in the t-matrix approximation, equation (12), for several values of the electron–impurity matrix element V_i, except for the results given by filled circles which were obtained in the Born approximation (the same as the solid curve in figure 3). s-wave symmetry is assumed and the on-site Coulomb repulsion $U = 0$ except for the results given by squares where U is set equal to half the bandwidth.

results are shown in figure 4 for $T_J = 90$ meV. We plot T_c as a function of the in-plane impurity concentration n_i for several values of the impurity scattering potential parameter V_i. Note that for $V_i = t = 250$ meV the t-matrix approximation (solid line) and the Born approximation (dots) give very similar results, as one would expect in the limit of small V_i (see equations (11) and (12)). Increasing V_i leads to a more rapid suppression of T_c with increasing impurity concentration, and the unitary limit is reached by $V_i = 6t$–$8t$ with $U = 0$. Note, however, the change in curvature of T_c versus n_i as V_i is increased. This trend was not found in the weak-coupling calculation of Bang [25] in crossover from the Born limit to the unitary limit. However, the overall rate of suppression of the transition temperature with increasing disorder that we find in the unitary limit is comparable to the rate found by Bang [25] for $\lambda = 0.5$ (with our $N(E_F) = 1.16 \times 10^{-3}$ states meV^{-1}/(cell spin) the impurity concentration $n_i = 0.1$ per cell corresponds to the impurity scattering rate in the unitary limit $\Gamma_i \equiv n_i/(\pi/N(E_F)) = 27$ meV). We also obtained steplike features in the T_c-curves in the unitary limit which we are not able to associate with any particular feature of the model and/or the numerical procedure used. The experiments [7–10] in general did not produce the data on the very fine scale over which we observe the steps, and only in [8] was there an attempt to interpret fine features of the observed dependence of

T_c for $Y_{1-x}Pr_xBa_2Cu_4O_8$ on the Pr concentration. It should be kept in mind that only the experiment of Tolpygo *et al* [10] addresses specifically the in-plane defects in $YBa_2Cu_3O_{6+x}$ at the fixed carrier concentration to which our model calculations apply. The most important aspect of figure 4 is that it illustrates the profound effect of the Coulomb interaction on the dependence of T_c on the concentration of in-plane impurities. For $U = 4t$ (half the bandwidth) the solid curve in figure 4 obtained for $V_i = t$ in the t-matrix approximation is pushed down to the line given by squares. The decrease in T_c for $U = 4t$ is about 5 K per 1% of in-plane defects, similar to the value found by Monthoux and Pines [12] for $V_i = t$ in the model of spin-fluctuation-induced superconductivity and d-wave paring, and to the value measured by Tolpygo *et al* [10]. Moreover, we found that for this choice of parameters ($\lambda = 0.48$, $U = 4t = 1$ eV) switching off the interlayer pair tunnelling reduces the transition temperature from 84.5 K (for $T_J = 90$ meV) to 1.6 K for $n_i = 0$. This illustrates the remarkable effect of the interlayer pair tunnelling mechanism on the enhancement of the T_c.

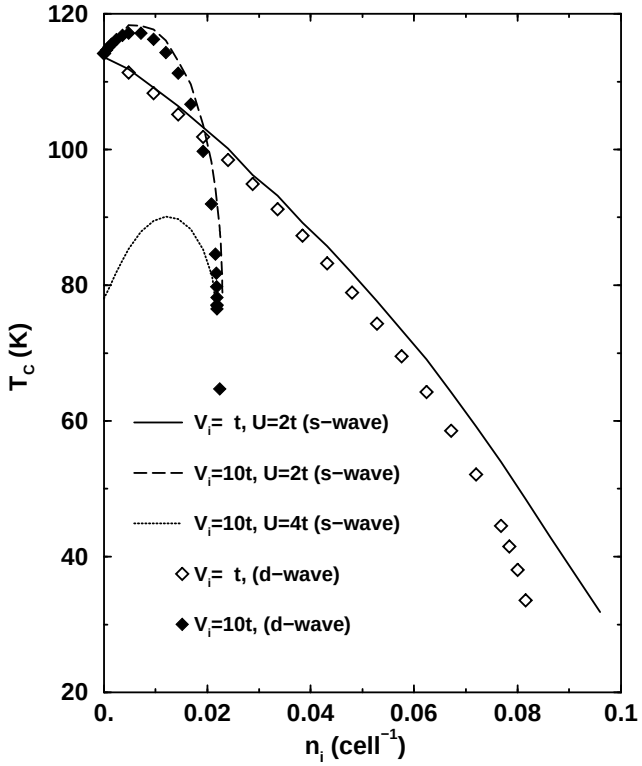

Figure 5. The dependence of T_c on the concentration n_i of in-plane impurities for $T_J = 90$ meV and for the anisotropic electron–phonon coupling model (33) (the same value of $|g|^2$ was used as in figures 3 and 4) calculated in the t-matrix approximation, equation (12), for the electron–impurity matrix element V_i set equal to either t or $10t$ (the unitary limit). The assumed symmetry of the gap is indicated in the brackets and the value of the on-site Coulomb repulsion U is indicated in the key. For $d_{x^2-y^2}$ symmetry of the gap, U drops out; see equation (10).

Next, we turn to the anisotropic model of the electron–phonon coupling function, equation (33). The results for $T_J = 90$ meV using the t-matrix approximation are shown in figure 5. As we have mentioned in the introduction, we were not able to obtain a finite

transition temperature assuming $d_{x^2-y^2}$ symmetry of the pairing self-energy for $T_J = 0$ down to the lowest temperature that we could consider using the $\boldsymbol{k}$-space method (about 20 K). However, with $T_J = 90$ meV we obtained a transition temperature of 114 K assuming $d_{x^2-y^2}$ symmetry of the gap for $n_i = 0$. It is interesting that the s-wave case with $U = 2t$ and the $d_{x^2-y^2}$-wave case (the on-site Coulomb repulsion drops out; see equation (10)) give quite a similar dependence of T_c on n_i for both $V_i = t$ and $V_i = 10t$. The results obtained for $V_i = t$ are similar to the experimental results on $YBa_2Cu_3O_{6+x}$ with in-plane oxygen defects [10], although we find that the squares in figure 4 more closely resemble the experimental data at the highest values of n_i where the data seem to fall on a curve that becomes less steep as n_i is increased. In the unitary limit $V_i = 10t$ the T_c-curves initially rise with increasing n_i and then precipitously drop. There seems to be a common threshold n_i beyond which superconductivity disappears for both the s-wave pairing with either $U = 2t$ or $U = 4t$ and the $d_{x^2-y^2}$-wave pairing. We have found a similar behaviour for s-wave pairing with $U = 4t$, $T_J = 90$ meV and $V_i = t$ (not shown here), except that the initial rise in T_c is much less pronounced and the threshold occurs at a higher value of n_i.

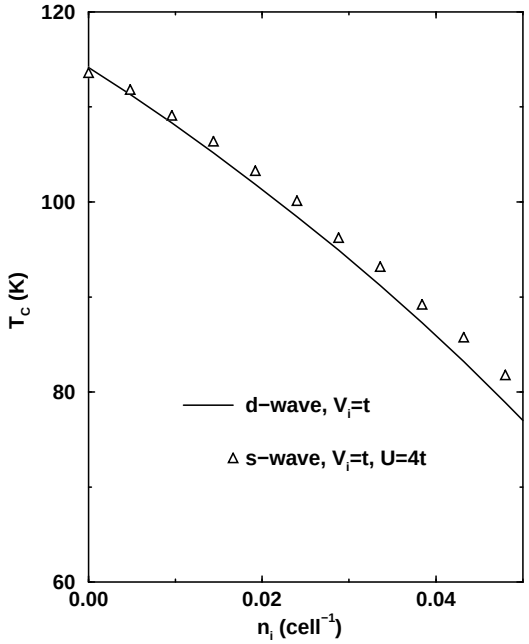

Figure 6. The dependence of T_c on the concentration n_i of in-plane impurities for $T_J = 90$ meV and for the anisotropic electron–phonon coupling model (33) (the same value of $|g|^2$ was used as in figures 3, 4 and 5) calculated in the t-matrix approximation, equation (12), for the electron–impurity matrix element $V_i = t$. The results for $d_{x^2-y^2}$ symmetry of the gap are given by the solid line and the results for s-wave symmetry are given by triangles. Note that as n_i increases the state with the highest T_c crosses over from $d_{x^2-y^2}$ symmetry to s-wave symmetry.

We would like to point out that with the electron–phonon coupling function given by equation (33) it is possible to have impurity-induced crossover from the $d_{x^2-y^2}$-wave state in a very pure system to the s-wave state at a higher impurity concentration; see figure 6. All of the interaction parameters for the two curves in figure 6 are the same. The only difference is that for the solid curve the $d_{x^2-y^2}$-symmetry of the pairing self-energy is assumed (in this

case the on-site Coulomb interaction drops out; see equation (10)), while for the triangles the s-wave symmetry is assumed. At a given impurity concentration the system will go into a state with a higher T_c in order to lower its free energy.

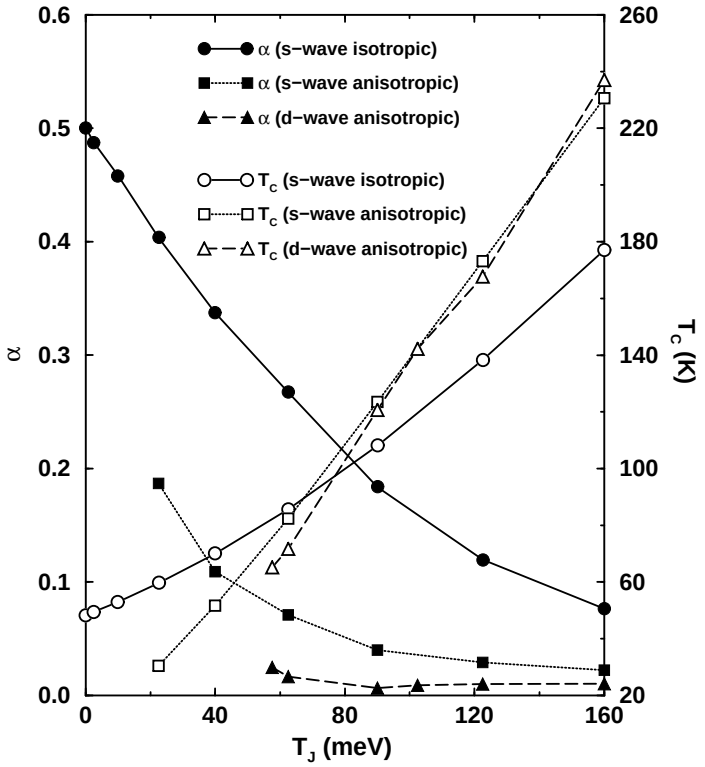

Figure 7. The isotope coefficient $\alpha = -\mathrm{d}\ln T_c/\mathrm{d}\ln M$ associated with the oxygen optical mode at 500 cm^{-1} and the corresponding T_c as functions of the interlayer pair tunnelling strength $T_J = t_\perp^2/t$. In all cases the on-site Coulomb repulsion U is equal to zero. The results obtained with the isotropic electron–phonon coupling model (32) are labelled as (s-wave isotropic). The results obtained with the anisotropic electron–phonon coupling model (33) are labelled as (s-wave anisotropic) or as (d-wave anisotropic) depending on whether s-wave or $\mathrm{d}_{x^2-y^2}$-wave symmetry is assumed, respectively. The value of $|g|^2$ is the same as in figures 3–6, leading to $\lambda = 0.48$ in the isotropic case.

3.2. The isotope effect associated with the in-plane oxygen optical mode

We have examined the isotope effect associated with the optical phonon which mediates the in-plane interaction. In the original work of Chakravarty *et al* it was suggested that the interlayer pair tunnelling mechanism could explain a small isotope effect in high-T_c copper oxide superconductors simply because in the interlayer tunnelling model the most important pairing process is associated with the pair tunnelling. Our results for the isotope exponent $\alpha = -\mathrm{d}\ln T_c/\mathrm{d}\ln M$ associated with the optical mode at Ω_E are shown in figure 7. In the same figure we give the corresponding transition temperatures. The impurity scattering was set equal to zero and the results for s-wave symmetry were obtained for the on-site Coulomb repulsion U equal to zero. Note that for the isotropic model of electron–phonon interaction, equation (32), we get the classical result $\alpha = 0.5$ for $T_J = 0$. In the same

model $T_J = 90$ meV gives $T_c = 108$ K and $\alpha = 0.18$. Turning on the on-site Coulomb repulsion to $U = 4t$ (half the bandwidth) reduces the transition temperature to $T_c = 84.5$ K and the isotope exponent to $\alpha = 0.05$ (not shown in figure 7)—a value approximately equal to what is found for the oxygen isotope effect in high-T_c Y–Ba–Cu–O systems [26]. In the site-selective oxygen isotope experiments of Nickel *et al* [27], where only the oxygen in copper–oxygen planes is replaced by a heavier isotope, a small negative isotope effect was observed with the partial isotope exponent $\alpha = -0.01 \pm 0.004$—close to the resolution limit [26]. Subsequently, the site-selective oxygen isotope experiments performed by Zech *et al* [28] established that more than 80% of the total (positive) oxygen isotope effect is associated with the copper–oxygen planes, in agreement with our calculation. For anisotropic electron–phonon interaction, equation (33), and assuming s-wave symmetry of the gap, we generally get lower values of α than in the isotropic case. For $T_J = 90$ meV and $U = 0$ the transition temperature is 123 K and $\alpha = 0.04$. Turning on $U = 4t$ reduces the T_c to 78 K and increases the isotope exponent to $\alpha = 0.08$. For $d_{x^2-y^2}$ symmetry of the gap we obtain very small positive values of α—probably smaller than the experimental resolution [26].

4. Conclusions

We have generalized the interlayer pair tunnelling model of Anderson and co-workers to include the retardation effects associated with in-plane interactions. Through numerical solutions of the T_c-equations for a model in which electrons couple to an optical phonon at 500 cm^{-1} (i.e. 62 meV) we found, without trying to fit the experiments, that a reasonable choice for the band parameters ($t = 250$ meV, $t'/t = -0.45$), band filling factor (0.75 electrons per cell), electron–phonon coupling ($\lambda = 0.48$), on-site Coulomb repulsion ($U \approx$ the bandwidth), and the interlayer pair tunnelling strength ($t_\perp = 0.15$ eV) results in surprisingly good agreement with the experiments on both a T_c-suppression by in-plane oxygen defects [10] and the oxygen isotope effect [26, 28] in $YBa_2Cu_3O_{6+x}$. The best agreement is found for the isotropic model of the electron–phonon coupling function with $U = 4t$ which leads to the T_c-suppression rate of about 5 K per 1% of the in-plane defects (with the impurity matrix element $V_i = t$) and to the oxygen isotope exponent $\alpha = 0.05$. This case also best illustrates the importance of the interlayer pair tunnelling process in raising the transition temperature, since reducing $t_\perp$ from 0.15 eV (i.e. $T_J = 90$ meV) to zero decreases the T_c from 84.5 K to 1.6 K. We also found that for the anisotropic form of the electron–phonon coupling proposed by Song and Annett [15], equation (33), the interlayer pair tunnelling can stabilize the superconducting state with $d_{x^2-y^2}$ symmetry at a high T_c. This stabilization occurs because the pair tunnelling contribution to the pairing self-energy is local in $\boldsymbol{k}$. Moreover, it is possible to have impurity-induced crossover from the $d_{x^2-y^2}$ state in a 'perfect' sample to the s-wave state at a higher concentration of defects. This is illustrated in figure 6 for $T_J = 90$ meV and U equal to a quarter of the bandwidth, but we have also found examples of such a crossover for other values of T_J and U.

Acknowledgments

We would like to thank S K Tolpygo for useful discussions, and Professor J P Frank for pointing out to us reference [28]. This work was supported by the Natural Sciences and Engineering Research Council of Canada.

References

[1] Wheatly J M, Hsu T C and Anderson P W 1988 *Phys. Rev.* B **37** 5897
[2] Chakravarty S, Sudbø A, Anderson P W and Strong S 1993 *Science* **261** 337
[3] Sudbø A, Chakravarty S, Strong S and Anderson P W 1994 *Phys. Rev.* B **49** 12 245
[4] Sudbø A 1994 *Physica* C **235–240** 126
[5] Sudbø A 1994 *J. Low Temp. Phys.* **97** 403
[6] Scalapino D J 1969 *Superconductivity* vol 1, ed R D Parks (New York: Dekker) pp 449–560
[7] Dynes R C 1994 *Solid State Commun.* **92** 53
Sun A G, Paulius L M, Gajewski D A, Maple M B and Dynes R C 1994 *Phys. Rev.* B **50** 3266
[8] Agrawal S K, Lal R, Awans V P S, Pandey S P and Narlikar A V 1994 *Phys. Rev.* B **50** 10 265
[9] Fukuzumi Y, Mizuhashi K, Takenaka K and Uchida S 1996 *Phys. Rev. Lett.* **76** 684
[10] Tolpygo S K, Lin J-Y, Gurvitch M, Hou S Y and Phillips J M 1996 *Phys. Rev.* B **53** 12 454
[11] Radtke R J, Levin K, Schüttler H-B and Norman M R 1993 *Phys. Rev.* B **48** 653
[12] Monthoux P and Pines D 1994 *Phys. Rev.* B **49** 4261
[13] Chakravarty S and Anderson P W 1994 *Phys. Rev. Lett.* **72** 3859
[14] Sudbø A 1995 *Phys. Rev. Lett.* **74** 2575
[15] Song J and Annett J F 1995 *Phys. Rev.* B **51** 3840 (erratum **52** 6930)
[16] Andersen O K, Liechtenstein A I, Jepsen O and Paulsen F 1996 *J. Phys. Chem. Solids* **56** 1573
[17] Schrieffer J R 1964 *Theory of Superconductivity* (New York: Benjamin)
[18] Allen P B and Mitrović B 1982 *Solid State Physics* vol 37, ed H Ehrenreich, F Seitz and D Turnbull (New York: Academic) pp 1–92
[19] For details see, for example,
Kostur V N and Mitrović B 1994 *Phys. Rev.* B **50** 12 774
Kostur V N and Mitrović B 1995 *Phys. Rev.* B **51** 6064
and the references therein.
[20] For details see, for example,
Höhn T and Mitrović B 1994 *Z. Phys.* B **93** 173
and the references therein.
[21] Abrikosov A A, Gor'kov L P and Dzyaloshinsky I Ye 1965 *Quantum Field Theoretical Methods in Statistical Physics* (New York: Pergamon)
[22] Lehmann G and Taut M 1972 *Phys. Status Solidi* b **54** 469
[23] Gentzsch W 1984 *Vectorization of Computer Programs with Applications to Computational Fluid Dynamics* (Braunschweig: Vieweg) pp 120–1
[24] Serene J W and Hess D W 1991 *Phys. Rev.* B **44** 3391
[25] Bang Y 1995 *Phys. Rev.* B **52** 1279
[26] Frank J P 1994 *Physical Properties of High Temperature Superconductors IV* ed D M Ginsberg (Singapore: World Scientific) pp 189–293 and references therein
[27] Nickel J H, Morris D E and Ager J W 1993 *Phys. Rev. Lett.* **70** 81
[28] Zech D, Keller H, Conder K, Kaldis E, Liarokapis E, Poulakis N and Müller K A 1994 *Nature* **397** 681